Review of Scientific Instruments

Setup for polarized neutron imaging using *in situ* ^{3}He cells at the Oak Ridge National Laboratory High Flux Isotope Reactor CG-1D beamline

Cite as: Rev. Sci. Instrum. **88**, 095103 (2017); https://doi.org/10.1063/1.5001525
Submitted: 20 December 2016 . Accepted: 24 August 2017 . Published Online: 12 September 2017

I. Dhiman, Ralf Ziesche, Tianhao Wang, Hassina Bilheux, Lou Santodonato, X. Tong, C. Y. Jiang, Ingo Manke, Wolfgang Treimer, Tapan Chatterji, and Nikolay Kardjilov

Setup for polarized neutron imaging using *in situ* ^{3}He cells at the Oak Ridge National Laboratory High Flux Isotope Reactor CG-1D beamline

I. Dhiman,[1,a)] Ralf Ziesche,[2,3] Tianhao Wang,[1] Hassina Bilheux,[1,a)] Lou Santodonato,[1] X. Tong,[1,4] C. Y. Jiang,[1] Ingo Manke,[2] Wolfgang Treimer,[2] Tapan Chatterji,[5] and Nikolay Kardjilov[2]

[1]*Neutron Science Directorate, Oak Ridge National Laboratory, Oak Ridge, Tennessee 37831, USA*
[2]*Helmholtz Centre Berlin for Materials and Energy, D-14109 Berlin, Germany*
[3]*Department of Chemical Engineering, University College London, Torrington Place, London WC1E 7JE, United Kingdom*
[4]*Department of Physics & Astronomy, The University of Tennessee, Knoxville, Tennessee 37996, USA*
[5]*Institute Laue-Langevin, 38042 Grenoble Cedex, France*

(Received 20 December 2016; accepted 24 August 2017; published online 12 September 2017)

In the present study, we report a new setup for polarized neutron imaging at the ORNL High Flux Isotope Reactor CG-1D beamline using an *in situ* ^{3}He polarizer and analyzer. This development is very important for extending the capabilities of the imaging instrument at ORNL providing a polarized beam with a large field-of-view, which can be further used in combination with optical devices like Wolter optics, focusing guides, or other lenses for the development of microscope arrangement. Such a setup can be of advantage for the existing and future imaging beamlines at the pulsed neutron sources. The first proof-of-concept experiment is performed to study the ferromagnetic phase transition in the Fe_3Pt sample. We also demonstrate that the polychromatic neutron beam in combination with *in situ* ^{3}He cells can be used as the initial step for the rapid measurement and qualitative analysis of radiographs. *Published by AIP Publishing.* [http://dx.doi.org/10.1063/1.5001525]

INTRODUCTION

Polarized neutron beam is a unique probe for the investigation of magnetic materials, due to their magnetic moment, charge neutrality, and the capability to penetrate deep inside the bulk samples. Neutrons have spin and thus are sensitive to the magnetic field distribution in and around the sample, such as in superconducting and ferromagnetic materials.[1–12] Polarized neutrons passing through an inhomogeneous magnetic field experience different Larmor precessions, dependent on the magnetic field strength and path integral through the sample. This path-dependent neutron spin rotation can be analyzed by a neutron spin analyzer placed after the sample. Polarized neutron imaging can be used to visualize the magnetic field distribution in the bulk of a sample to obtain three-dimensional information in real space. Visualization of magnetic phase transitions, as a function of magnetic field strength and/or temperature, can contribute towards the understanding of underlying physics involved at the microscopic length scales, yielding a deeper insight into the magnetic phase transitions. However, one of the major challenges in the field of neutron imaging is the spatial resolution in order to resolve the magnetic domains and structures, within micrometric length scale resolution. Moreover, the measurement duration has to be taken into consideration, particularly when performing tomography to visualize the magnetic fields in three dimensions.

In order to obtain high spatial resolution, one needs to maintain the sample-to-detector distance as small as possible and overcome polarizer devices based on neutron reflection (e.g., solid state benders), thereby reducing the geometric blurring effects. This is the reason to focus our efforts towards the use of spin filter cells, with *in situ* polarization of the ^{3}He gas. The ^{3}He polarizer/analyzer can also be used over a large neutron wavelength range, thus they are well suited for a polychromatic beam. Additionally, the neutron trajectory is not modified with ^{3}He cells, in contrast to solid state benders. A detailed comparison between ^{3}He polarizer and solid state benders has been described by Dawson *et al.*[8] This configuration is very beneficial for high-resolution applications because of the minimal perturbation of the neutron beam passing through the ^{3}He cells and for future experiments performed at pulsed neutron sources [e.g., spallation neutron source (SNS), Japan proton accelerator research complex (J-PARC), science and technology facilities council (ISIS Neutron) and the future european spallation source (ESS)] where a Time-Of-Flight (TOF) technique can be applied. The combination of polarized neutrons with the TOF technique allows for the measurements of the spin precession angle of the neutrons for different wavelengths. This approach can be used for the development of algorithms towards the quantification of magnetic fields, which can be further extended towards magnetic vector tomography.

In addition, the *in situ* ^{3}He cells are very important components, when used in combination with optical devices like Wolter optics,[13,14] focusing guides,[15,16] or other types of neutron lenses[17] for the formation of a neutron beam. Using this

[a)]Authors to whom correspondence should be addressed: dhimani@ornl.gov and bilheuxhn@ornl.gov

setup, the neutron beam with high divergence (e.g., transported through the neutron guide) can be polarized by the ^{3}He polarizer without geometrical distortions and blurring effects. After the interaction with the magnetic field within the sample, the polarized neutron beam is passed through the ^{3}He analyzer and focused by a neutron optical lens (e.g., Wolter optics or focusing guide) on the detector plane, providing a magnified sample's image. The advantage of this configuration is that the distance between the sample and detector does not influence the image resolution and the dimension of the analyzer is not of importance.

Our aim is to implement polarized neutron imaging at the High Flux Isotope Reactor (HFIR) CG-1D neutron imaging beamline. We have recently carried out polarized imaging experiments with the CG-1D polychromatic and monochromatic beams using the ^{3}He polarizer and analyzer. The comparison between measurements with monochromatic and polychromatic neutron beams shows that for low magnetic fields, the visibility with polychromatic neutrons is sufficient to visualize the effect of the magnetic field. This helps us to improve the acquisition time and permit data acquisition on the order of few minutes rather than 10 s of minutes with the monochromatic beam. Therefore, the polychromatic neutron beam can be utilized for mapping the transition temperatures or to visualize the effect of sample inhomogeneities on the magnetic transitions.

POLARIZED IMAGING SETUP AT THE CG-1D BEAMLINE

Polarized neutron imaging measurements are carried out on the CG-1D beamline, located at the end of a cold neutron guide. The neutron wavelength, λ, ranges from 0.8 to 6.0 Å, with a peak neutron intensity of 2.2×10^6 (n/cm^2)/s for λ = 2.6 Å. The distance from the aperture to detector is L = 6.59 m, and the aperture size is D = 3.3 mm, with L/D of approximately 2000. The detailed description of the instrument is provided elsewhere.[18] Using the aperture size of 3.3 mm and a sample-to-detector distance of 60 cm, the spatial resolution at the sample position is approximately 350 μm. A monochromatic beam with the wavelength of 2.53 Å is set up by using a double-crystal monochromator device, utilizing two highly oriented pyrolytic graphite (HOPG) crystals with a mosaicity of 0.5°.

Neutron depolarization effects are detected using a 100 μm thick ^{6}LiF/ZnS scintillator attached to a CCD system (Andor® iKon-L 936 model). The field-of-view (FOV) for this CCD system is ~7.4 cm × 7.4 cm. However, for the current setup, the FOV is limited by the dimensions of the polarizer and analyzer. Samples are mounted in Al holders and cooled/warmed using a closed cycle helium refrigerator (CCR), with an Al vacuum shroud and heat shields for neutron windows.

The *in situ* ^{3}He polarizer/analyzer used in the current setup is based on the spin-exchange optical pumping (SEOP) mechanism. To achieve a uniform magnetic field for the SEOP process, the whole system is built around a μ-metal shielded solenoid. To maintain the proper temperature of 200°C for the ^{3}He cell, it is kept inside a cylindrically shaped oven. A sapphire window on each side of the oven is used for the laser and polarized neutron beam to go through. Also the end-compensated solenoid is mounted to maintain the uniform magnetic field. A QPC 200 W fiber-coupled laser with a spectral linewidth of 0.35 nm is utilized for optical pumping in this system. A nuclear magnetic resonance (NMR) based technique is used to monitor the ^{3}He polarization and perform

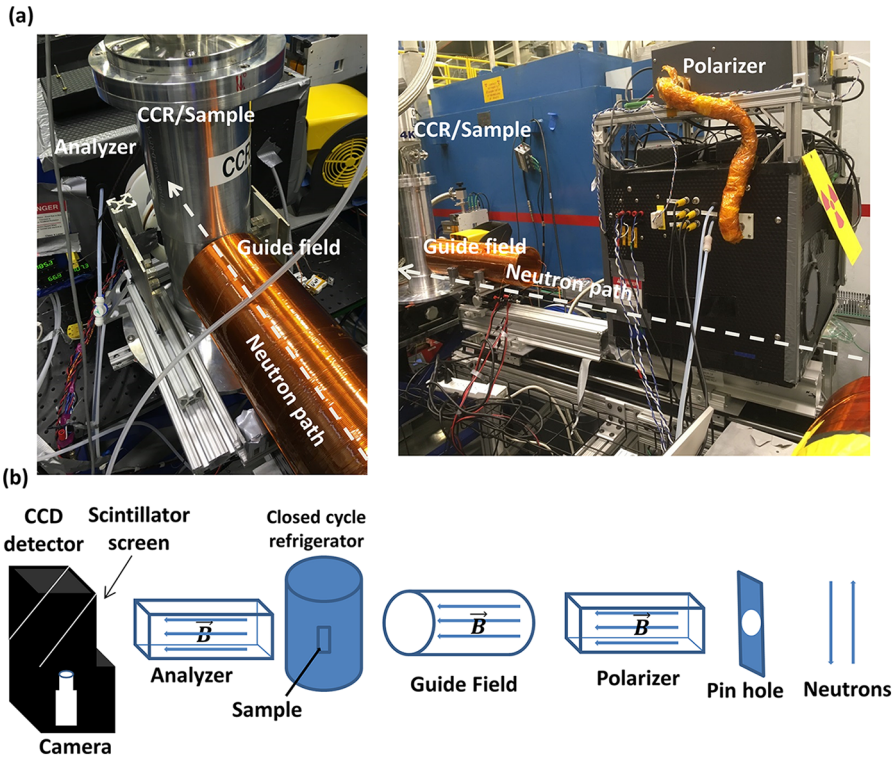

FIG. 1. (a) Two different photographic views of the setup and (b) schematic of the instrument setup for polarized neutron imaging measurements at the ORNL HFIR CG-1D neutron imaging beamline. The guide field was switched off during the measurement.

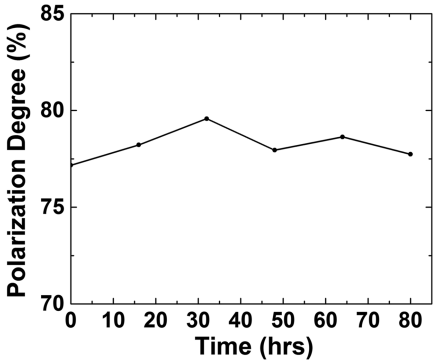

FIG. 2. Neutron polarization degree as a function of time.

flipping operation. In particular, to flip the ^{3}He spin and in turn the neutron spin polarization, the adiabatic fast passage NMR method is applied. To determine the absolute ^{3}He polarization, electron paramagnetic resonance measurements are also carried out.

The experimental setup and schematic for this measurement is depicted in Fig. 1.[19,20] The *in situ* polarizer box is 61 cm long along the beam direction with the cell inside of 7 cm length and 9 cm outer diameter dimensions and a pressure of 1.547 bars. In comparison to the *ex situ* ^{3}He polarizer/analyzer system, the *in situ* ^{3}He system utilizes continuous pumping during an experiment in order to maintain a constant ^{3}He polarization. The pressure and length of the ^{3}He gas is optimized to yield the best performance around the peak neutron intensity at a wavelength of 2.6 Å. The analyzer is an *in situ* system with a pressure of 1.47 bars, with 75 mm outer diameter and 100 mm length along the neutron beam path. The analyzer device has a length of 51 cm. To evaluate the initial degree of polarization, spin up and spin down measurements are performed. The obtained degree of neutron beam polarization was up to 80% (shown in Fig. 2), stable within the range of 2%-3% over 80 h.

The measured transmission intensity using polarized neutrons is not only the contribution from the neutron spin interaction with the sample magnetic field but is also affected by the composition- and density-based conventional attenuation. Therefore, to remove the conventional attenuation contribution, all the radiographs are normalized with respect to the radiographs measured with no magnetic contribution. Image processing is done using ImageJ, wherein noise reduction is carried out using a median filter, and 4 × 4-pixel binning is used.[21]

RESULTS

The first proof of principle experiment of the system is performed by visualizing the uniform magnetic field inside a cylindrical coil as a function of current (19 mm inner diameter, 150 mm length, and 614 windings), placed perpendicular to the neutron path direction. Figures 3(a)–3(d) show normalized transmission polarized neutron radiographs of the cylindrical coil as a function of current, with 300 s of exposure time using a monochromatic beam. The magnetic field inside the coil is expected to be homogeneous and significantly stronger than the field around the coil.[2]

The incoming neutron spin is perpendicular to the coil magnetic field, and upon entering the sample, it starts the Larmor precession until exiting the coil. This neutron spin precession after interacting with the magnetic field distribution with respect to its initial spin state is analyzed. The neutron spin precession for a cylindrical coil having the homogeneous magnetic field distribution is only dependent on the neutron path length through the sample. For cylindrical geometry, the neutron path length is maximum along the diameter and reduces symmetrically as moving towards the edges. The evolution of the fringe pattern (magnetic in nature) as a result of position dependent rotation of neutrons spin is expected, shown in Figs. 3(a)–3(d) as a function of current. As the current is increased, the magnetic field line density (i.e., fringe density) inside the sample is increased. This in turn modifies the precession of the neutron spin through the coil. This displays [Figs. 3(a)–3(d)] the change in neutron spin rotation (reduced transmission) after interacting with the magnetic field present inside the coil. Both the polarizer and analyzer are set up in such a way that mostly up spin neutrons are transmitted. The percentage of up spin neutrons transmitted through the polarizer/analyzer is dependent on the polarization efficiency. As a result, for the up spin configuration of the polarizer and analyzer, maximum transmission intensity is measured on the detector. As the analyzer is set up to accept up spin neutrons, deviation of neutron spins from this orientation causes reduction in transmission, with the minimum for a complete π-spin flip. Further, no significant change in neutron spin rotation is observed around the sample, attributable to a much weaker magnetic field, also remarked by Dawson *et al.*[2]

To better visualize the change in transmission intensity as a function of current, the normalized transmission plot for the selected region of interest along the coil diameter with the maximum neutron path length through the sample [as indicated in Fig. 3(a), by solid white lines] is shown in Fig. 4.

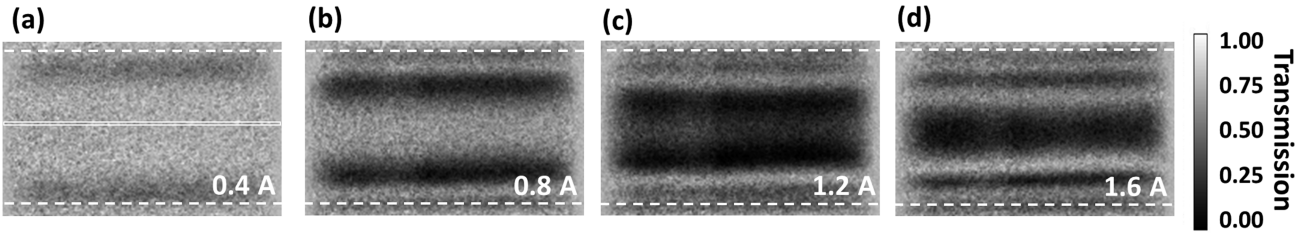

FIG. 3. Polarized transmission neutron radiographs of a cylindrical coil with inner diameter = 19 mm, length = 150 mm, and 614 windings, measured as a function of current: (a) 0.4 A, (b) 0.8 A, (c) 1.2 A, (d) 1.6 A, using monochromatic neutron beam. Dotted lines in the radiographs indicate the coil diameter, while the solid white lines in (a) shows the ROI used for Fig. 4.

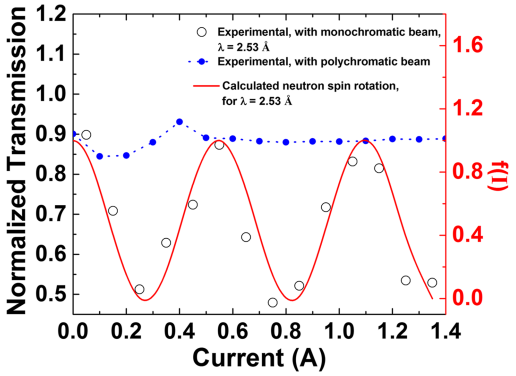

FIG. 4. Transmission plot for a selected region of interest [solid white lines in Fig. 3(a) show the ROI] inside the coil as a function of current, shown with black circles. For comparison, the calculated curve is also plotted for a monochromatic neutron wavelength of 2.53 Å, shown as a continuous red line. Also blue solid points in the graph depict the measurements carried out using a polychromatic neutron beam.

For comparison, the calculated curve [based on Eq. (4)] is also plotted for a monochromatic neutron beam, at a wavelength of 2.53 Å and with the assumption of 100% polarization.

The mathematical steps followed towards the calculation of neutron spin rotation between up (+1) and down (−1) as a function of current for a cylindrical coil using a monochromatic beam are as described below.

When the neutron spin interacts with a magnetic field **B**, having a non-zero component perpendicular to the neutron spin vector, it begins to perform the Larmor precession with the frequency ω_L (= $\gamma_L \times$ B). The rotation angle, ϕ, of the neutron spin is dependent on time, t, needed for neutrons to pass through the magnetic field. This spin rotation, ϕ, can be calculated as[1]

$$\phi = \omega_L t = \gamma_L B t = \frac{\gamma_L}{v_L} \int_{path} B ds = \frac{\gamma_L m}{h} B s \lambda, \tag{1}$$

where $v_L \left(= \frac{h}{m\lambda},\ h\ is\ Planck's\ constant\right)$ is the neutron velocity, m is the neutron mass, s is the path integral in the field, γ_L is the gyromagnetic ratio of neutrons, and λ is the neutron wavelength. In the present case, we assume that $B = (B_x, B_y, B_z) = (0, 0, B_z)$. Therefore, ϕ is proportional to B and λ.

Further, the number of 2π spin precessions, n, as a function of B is given by

$$n(B) = \frac{\gamma_L}{2\pi v_L} B s = \frac{\gamma_L m \lambda s}{2\pi h} B. \tag{2}$$

For a cylindrical coil, the applied electric current creates a homogeneous magnetic field **B**. Magnetic field (**B**) strength variation as a function of electric current (I), for a given length (l), and numbers of windings (N) for a cylindrical coil is given by $B = \mu_0 \frac{N}{l} I$, where μ_0 is the permeability of vacuum and is given by $\mu_0 = 4\pi \times 10^{-7}$ V s/(Am).

Therefore,

$$n(I) = \frac{\gamma_L m \lambda s}{2\pi h} \left[\mu_0 \frac{N}{l} I\right]. \tag{3}$$

Finally, the neutron spin precession (between up and down) function $f(I) = \cos[2\pi \cdot n(I)]$ with a varying current, as shown in Fig. 4, is given by

$$f(I) = \cos\left(\frac{\gamma_L m \lambda s}{h} \mu_0 \frac{N}{l} I\right). \tag{4}$$

In Fig. 4, the calculated and experimental data exhibit a similar trend. Also, similar behavior (as shown in Fig. 4) in the transmission intensity curves with a varying current for different positions of the coil is observed. For cylindrical geometry moving away from the coil diameter, the neutron path length through the coil is reduced. This would cause a decrease in the number of neutron spin rotations for the current values between 0 and 1.8 A. Further, we also carried out similar measurements using the polychromatic neutron beam, with an exposure time of 60 s. Comparison between polychromatic and monochromatic measurements is shown in Fig. 4. At low current values below 0.5 A, the polychromatic data show a visibility of 3%. This indicates that the polychromatic beam can be used as the initial step for the rapid measurement and qualitative analysis of radiographs, particularly at low current (magnetic field) values. At higher current values (>0.5 A), the polychromatic neutron beam is completely de-phased. As a result, no change in the transmission value is expected, reaching a plateau. The advantage of the polychromatic neutron beam towards the qualitative understanding of magnetic phase transitions has been reported by Schulz *et al.*[11] It is interesting to point out that the periodicity of the transmission curves is different for the polychromatic and monochromatic measurements (Fig. 4). Wherein, the second maximum in Fig. 4 for the polychromatic beam (at 0.4 A) is slightly shifted in comparison to the monochromatic beam (at 0.55 A). This can be explained with a different mean wavelength spectrum for the polychromatic beam, as against a monochromatic beam with wavelength 2.53 Å.

Following the verification of the experimental setup using the cylindrical coil, ferromagnetic Fe_3Pt is investigated using a polychromatic beam to demonstrate the polarized neutron imaging capability at the CG-1D beamline.

The ferromagnetic phase transition of an Iron Platinum (Fe_3Pt)-based single crystal is measured using a polychromatic polarized neutron beam to study the temperature dependent evolution of the ferromagnetic phase transition and possible domain structures. The single crystal with dimensions of $10 \times 3 \times 20$ mm^3 is grown by the Bridgman method. The Fe-Pt alloys are of interest because of their interesting physical properties such as invar effect (absence of thermal expansion), giant magnetostriction, shape memory effect, and potential application in the field of magneto-optic recording media.[22–25] The alloys of $Fe_{1x}Pt_x$ series can be both stoichiometric and non-stoichiometric with a varying degree of order. Among this series, the most stable invar region exists for an ordered Fe_3Pt alloy with a Cu_3Au type crystal structure. The magnetic properties of Fe_3Pt depend on this structural order. In the ordered state Fe_3Pt, ferromagnetic transition temperature goes up to 435 K, while in the disordered state, ferromagnetic T_C drops down to 260 K.[26–28]

Polarized neutron radiographs for the Fe_3Pt sample as a function of temperature, with an exposure time of 600 s while warming the sample from 400 K to 450 K, are shown in Fig. 5. The radiographs depicted in Fig. 5 are normalized

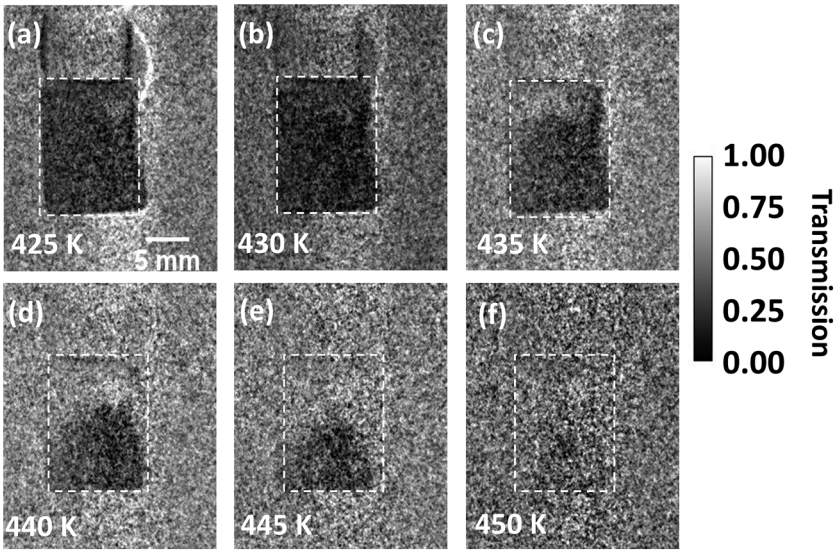

FIG. 5. Polarized neutron radiographs for Fe_3Pt ($10 \times 3 \times 20$ mm^3) as a function of temperature, with an exposure time of 600 s: (a) 425 K, (b) 430 K, (c) 435 K, (d) 440 K, (e) 445 K, (f) 450 K. Measurements are carried out while heating the sample from 425 K to 450 K. White dashed boxes show the sample area. Contrast of the radiographs is enhanced artificially to improve the visualization of magnetic effects inside the sample.

with respect to the one measured in the paramagnetic state, i.e., above 450 K. In the ferromagnetic phase below the Curie temperature (T_C), i.e., at 425 K, the depolarization of the neutron beam is clearly illustrated in Fig. 5(a). The presence of magnetic domains below T_C causes neutron spin precessions, hence the decreased transmission in the radiographs. As the temperature is increased, this effect is continuously reduced, as illustrated in Figs. 5(b)–5(f). At 450 K, the sample reaches a paramagnetic state (magnetically disordered). Thus, neutron up spin orientation is not affected anymore, and since both the polarizer and analyzer accept up spins, the transmission increases, as seen with the disappearance of dark regions of reduced transmission, in Fig. 5(f). Inhomogeneity in the neutron beam depolarization inside the sample as temperature is increased closer to T_C is also observed in Fig. 5. This behavior may suggest a temperature gradient within the sample or the sample is stoichiometrically inhomogeneous, leading to the variation in Curie temperatures in different parts of the crystal. It is also possible that non-uniform depolarization effects visualized as a function of temperature in Fe_3Pt are a combination of temperature gradient inside CCR and sample inhomogeneities.

CONCLUSION

A new setup for imaging with polarized neutrons based on spin filters with *in situ* polarized ^{3}He was used to conduct proof-of-concept experiments at the ORNL HFIR CG-1D beamline. The obtained neutron beam polarization degree with this setup was up to 80%, stable within the range of 2%-3% over 80 h. The ferromagnetic phase transition in Fe_3Pt as a function of temperature was observed. A spatial resolution of 350 μm was achieved using a polychromatic neutron beam, permitting considerable reduction in measurement time in comparison with a monochromatic beam. In the present study, we also showed the possibility of visualizing magnetic phase transitions at low external magnetic fields using a polychromatic neutron. Further, we plan to refine the technique allowing higher spatial resolution and smaller exposure time, with a better polarizer/analyzer setup, reducing the sample-to-detector distance. The ultimate goal is to establish the polarized neutron imaging technique at ORNL and provide it to the user community which will help to gain better understanding of underlying phenomena in the field of magnetism and superconductivity.

ACKNOWLEDGMENTS

This research used resources at the High Flux Isotope Reactor, a DOE Office of Science User Facility operated by the Oak Ridge National Laboratory. This material is based on work supported by the Office of Basic Energy Sciences, U.S. Department of Energy. The team would like to thank the sample environment team for their help with the refrigerator.

This manuscript has been authored by UT-Battelle, LLC under Contract No. DE-AC05-00OR22725 with the U.S. Department of Energy. The United States Government retains and the publisher, by accepting the article for publication, acknowledges that the United States Government retains a non-exclusive, paid-up, irrevocable, worldwide license to publish or reproduce the published form of this manuscript or allow others to do so, for United States Government purposes. The Department of Energy will provide public access to these results of federally sponsored research in accordance with the DOE Public Access Plan (http://energy.gov/downloads/doe-public-access-plan).

[1]O. Halpern and T. Holstein, Phys. Rev. **59**, 960 (1941).
[2]M. Dawson, I. Manke, N. Kardjilov, A. Hilger, M. Strobl, and J. Banhart, New J. Phys. **11**, 043013 (2009).
[3]W. Treimer, J. Magn. Magn. Mater. **350**, 188 (2014).
[4]W. Treimer, O. Ebrahimi, N. Karakas, and R. Prozorov, Phys. Rev. B **85**, 184522 (2012).
[5]I. Dhiman, O. Ebrahimi, N. Karakas, H. Hoppner, R. Ziesche, and W. Treimer, Phys. Procedia **69**, 420 (2015).
[6]N. Kardjilov, I. Manke, M. Strobl, A. Hilger, W. Treimer, M. Meissner, T. Krist, and J. Banhart, Nat. Phys. **4**, 399 (2008).
[7]M. Schulz, A. Neubauer, S. Masalovich, M. Mhlbauer, E. Calzada, B. Schillinger, C. Peiderer, and P. Boni, J. Phys.: Conf. Ser. **211**, 012025 (2010).

[8]M. Dawson, N. Kardjilov, I. Manke, A. Hilger, D. Jullien, F. Bordenave, M. Strobl, E. Jericha, G. Badurek, and J. Banhart, Nucl. Instrum. Methods Phys. Res., Sect. A **651**, 140–144 (2011).
[9]C. P. Poole, Jr., H. A. Farach, R. J. Creswick, and R. Prozorov, *Superconductivity*, 2nd ed. (Academic Press, Amsterdam, 2007).
[10]R. P. Huebener, *Magnetic Flux Structures in Superconductors* (Springer-Verlag, New York, 2001).
[11]M. Schulz, A. Neubauer, P. Boeni, and C. Pfleiderer, Appl. Phys. Lett. **108**, 202402 (2016).
[12]A. S. Tremsin, N. Kardjilov, M. Strobl, I. Manke, M. Dawson, J. B. McPhate, J. V. Vallerga, O. H. W. Siegmund, and W. B. Feller, New J. Phys. **17**, 043047 (2015).
[13]B. Khaykovich, M. V. Gubarev, Y. Bagdasarova, B. D. Ramsey, and D. E. Moncton, Nucl. Instrum. Methods Phys. Res., Sect. A **631**, 98 (2011).
[14]D. Liu, D. Hussey, M. V. Gubarev, B. D. Ramsey, D. Jacobson, M. Arif, D. E. Moncton, and B. Khaykovich, Appl. Phys. Lett. **102**, 183508 (2013).
[15]N. Kardjilov, A. Hilger, M. Dawson, I. Manke, J. Banhart, M. Strobl, and P. Böni, J. Appl. Phys. **108**, 034905 (2010).
[16]N. Kardjilov, P. Böni, A. Hilger, M. Strobl, and W. Treimer, Nucl. Instrum. Methods Phys. Res., Sect. A **542**, 248 (2005).
[17]R. Bartmann, N. Behr, A. Hilger, and T. Krist, Nucl. Instrum. Methods Phys. Res., Sect. A **634**, S104 (2011).
[18]L. Santodonato, H. Z. Bilheux, B. Bailey, J. Bilheux, P. T. Nguyen, A. S. Tremsin, D. L. Selby, and L. Walker, Phys. Procedia **69**, 104 (2015).
[19]C. Y. Jiang, X. Tong, D. R. Brown, S. Chi, A. D. Christianson, B. J. Kadron, J. L. Robertson, and B. L. Winn, Rev. Sci. Instrum. **85**, 075112 (2014).
[20]X. Tong, C. Y. Jiang, V. Lauter, H. Ambaye, D. Brown, L. Crow, T. R. Gentile, R. Goyette, W. T. Lee, A. Parizzi, and J. L. Robertson, Rev. Sci. Instrum. **83**, 075101 (2012).
[21]C. A. Schneider, W. S. Rasband, and K. W. Eliceiri, Nat. Methods **9**, 671 (2012).
[22]T. Kakeshita *et al.*, Appl. Phys. Lett. **77**, 1502 (2000).
[23]H. Zeng, J. Li, J. P. Liu, Z. L. Wang, and S. Sun, Nature **40**, 395 (2002).
[24]K. Sumiyama, M. Shiga, Y. Kobayashit, K. Nishi, and Y. Nakamura, J. Phys. F: Met. Phys. **8**, 1281 (1978).
[25]M. Podgorny, Phys. Rev. B **43**, 11300 (1991).
[26]Y. Ishikawa, S. Onodera, and K. Tajima, J. Magn. Magn. Mater. **10**, 183 (1979).
[27]Y. Suzuki, H. Miyajima, G. Kido, N. Miura, and S. Chikazumi, J. Phys. Soc. Jpn. **50**, 817 (1981).
[28]K. J. Kim, S. J. Lee, T. A. Wiener, and D. W. Lynch, J. Appl. Phys. **89**, 244 (2001).